

Titre: Shock-fitting approach for calculating air pocket entrapment caused by full obstruction in closed conduit transient flow
Title:

Auteurs: Arman Rokhzadi, & Musandji Fuamba
Authors:

Date: 2020

Type: Article de revue / Article

Référence: Rokhzadi, A., & Fuamba, M. (2020). Shock-fitting approach for calculating air pocket entrapment caused by full obstruction in closed conduit transient flow. Journal of Hydraulic Engineering, 146(11), 04020078 (13 pages).
Citation: <https://doi.org/10.1061/%28asce%29hy.1943-7900.0001817>

Document en libre accès dans PolyPublie

Open Access document in PolyPublie

URL de PolyPublie: <https://publications.polymtl.ca/9305/>
PolyPublie URL:

Version: Version officielle de l'éditeur / Published version
Révisé par les pairs / Refereed

Conditions d'utilisation: CC BY
Terms of Use:

Document publié chez l'éditeur officiel

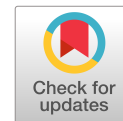
Document issued by the official publisher

Titre de la revue: Journal of Hydraulic Engineering (vol. 146, no. 11)
Journal Title:

Maison d'édition: American Society of Civil Engineers
Publisher:

URL officiel: <https://doi.org/10.1061/%28asce%29hy.1943-7900.0001817>
Official URL:

Mention légale: This work is made available under the terms of the Creative Commons Attribution 4.0 International license, <https://creativecommons.org/licenses/by/4.0/>.
Legal notice:



Shock-Fitting Approach for Calculating Air Pocket Entrapment Caused by Full Obstruction in Closed Conduit Transient Flow

Arman Rokhzadi, Ph.D.¹; and Musandji Fuamba, Ph.D., M.ASCE²

Abstract: This paper studies the ability of a Shock-Fitting approach in computing air pocket entrapments in a closed conduit transient flow, caused by suddenly blocking the downstream end. The flow is pressurized at the upstream, which detaches from the wall somewhere at the downstream after which a free surface flow develops. In this Shock-Fitting approach a pressurized flow is simulated by the rigid column model and the free surface flow is simulated by the Saint-Venant equations set. A transient region, which is characterized by the speed of the discontinuity, links these two flow regimes. The relevant governing equations of the rigid column model and the transient region are solved using the backward Euler temporal scheme and the Saint-Venant equations set is solved using the method of characteristics. It was found that this Shock-Fitting approach is able to predict the attenuation behavior as well as to calculate the flow variables more efficiently than the rigid column model and the modified Saint-Venant equations. By means of a linear stability analysis, it was shown that these improvements are provided by the speed of discontinuity in the transient region and the pressurized water column length. DOI: [10.1061/\(ASCE\)HY.1943-7900.0001817](https://doi.org/10.1061/(ASCE)HY.1943-7900.0001817). This work is made available under the terms of the Creative Commons Attribution 4.0 International license, <https://creativecommons.org/licenses/by/4.0/>.

Introduction

The ground level water and rainfall amounts are conducted through below-grade closed conduit systems, in which the flow regime is mostly a free surface flow. Disturbing boundary conditions, i.e., blockage or excessive amounts of discharge, may cause the free surface flow to change to a partially pressurized flow. Previous studies, either numerically or experimentally, e.g., Hamam and McCorquodale (1982), Cardle et al. (1989), and Li and McCorquodale (1999), indicated that a hydraulic instability may occur due to this transition, from free surface flow to partially pressurized flow, by which the air is trapped and undergoes compressions and expansions with high pressure values. Consequently, the air pocket could abruptly escape and result in damaging effects to structures as well as the public safety and health.

The Preissmann slot model, exemplified by the work of Cunge and Wegner (1964), has been used to simulate these transient flows; however, this model is unable to predict subatmospheric pressures. Furthermore, this hypothetical slot can result in spurious oscillations as shown by Trajkovic et al. (1999) and Vasconcelos et al. (2006). The two-components pressure approach (TPA), an alternative to the Preissmann slot, was proposed by Vasconcelos et al. (2006) and further studied by Vasconcelos and Wright (2007) and Vasconcelos and Marwell (2011) to overcome the inability of the Preissmann slot model in calculating subatmospheric

pressures. This approach can capture the relevant experimental data with a good agreement; however, it is subject to oscillatory behaviors, particularly, in presence of high pressure wave speeds (Bousso et al. 2013). The other shock capturing models, as of those studied by León et al. (2007), León (2007), and León et al. (2010), provide more accurate and reliable solutions since they are solved by finite volume methods, which preserve the conservation of mass and momentum. However, the main disadvantages of these models are that they are expensive and difficult to implement.

The rigid column (RC) model has attracted extensive attention as it is conceptually simple while it incorporates fundamental features of closed conduit transient flows. This lumped-pressure model is based on neglecting the water compressibility, which allows assuming a space-invariant velocity and acceleration, as those of Li and McCorquodale (1999, 2001) and Zhou et al. (2004).

Zhou et al. (2004) experimentally studied the air pocket entrapment in a rapidly filling partially pressurized flow in a dead-end pipe. They described the free surface flow section as tail water and they found it beneficial to reduce the induced air pressure.

Vasconcelos and Leite (2012), by using the RC model, experimentally and numerically investigated air pocket entrapments, caused by completely and partially closing a gate valve at the downstream. Subsequently, Hatcher et al. (2015) studied the same problem, experimentally and numerically, using the RC model as well as the modified Saint-Venant equations set (MSV). Both models predicted the solutions with reasonable tolerance of accuracy, except for the total valve closure in which both models significantly overestimated peak values as well as these models were unable to predict attenuation behaviors attributed to these transient flows. The results showed that in calculating cases with small initial air volume, the modified Saint-Venant equations set improves the accuracy compared to the RC model, while in calculating the cases with larger air volumes, both models perform similarly.

Tijsseling et al. (2019) used a rigid column model to solve, numerically and analytically, a pipe filling flow with a liquid supplied from a reservoir with varying elevations in which an air pocket is

¹Postdoctoral Researcher, Dept. of Civil, Geological and Mining Engineering, Polytechnique Montréal, C.P. 6079, succ. Centre-ville Montréal, QC, Canada H3C 3A7 (corresponding author). ORCID: <https://orcid.org/0000-0003-2009-1299>. Email: arman.rokhzadi@polymtl.ca

²Full Professor, Dept. of Civil, Geological and Mining Engineering, Polytechnique Montreal, C.P. 6079, succ. Centre-ville Montréal, QC, Canada H3C 3A7. Email: musandji.fuamba@polymtl.ca

Note. This manuscript was submitted on May 13, 2019; approved on June 15, 2020; published online on September 15, 2020. Discussion period open until February 15, 2021; separate discussions must be submitted for individual papers. This paper is part of the *Journal of Hydraulic Engineering*, © ASCE, ISSN 0733-9429.

allowed to be vented. They found that the result of their model is consistent with Martin (1996). Chaiko and Brinckman (2002) studied the air pocket entrapment in a pipe flow assuming two separate columns for the water and the air flows. For the water flow, they applied the water hammer equations, and for the air flow they solved the relevant momentum and continuity equations. To calculate the air flow, they studied two cases; in the first one, they assumed the air velocity varies along the pipe axis, called nonuniform compression, while in the second case, they neglected this variation, called uniform compression process. They also investigated whether the variation of the water length has any possible effect on the solutions. They concluded that for cases in which the air pocket volume is less than 5% of the total pipe volume the assumptions of the nonvarying water column length and uniform air compression are acceptable while for other cases the uniform air compression and time-varying water column length can capture all the essential features of the flow.

Shock-Fitting approaches allow using different governing equations for the pressurized and the free surface flows as indicated in numerous studies, e.g., Guo and Song (1990) and Fuamba (2002), and the air-water interface could be calculated using interpolation techniques. As indicated by Politano et al. (2007) and Bouso and Fuamba (2014), interpolations do not conserve the mass continuity and generate significant errors. Thus, using the mass and momentum conservation equations around the wave front improves the accuracy (Bouso and Fuamba, 2014).

Objectives

This paper studies a transient pressurized-free surface flow in a closed conduit, in which, by suddenly blocking the downstream end, an air pocket is entrapped causing a surge pressure to induce. Using a Shock-Fitting approach, the upstream pressurized flow is simulated by the rigid column model and the downstream free surface flow is simulated by the Saint-Venant equations and both flows are connected by a transient region that contains a discontinuity of the pressurized flow from the free surface flow.

Malekpour and Karney (2012) studied the rigid column model and found that the water column length has an influential impact on the maximum pressure head. In this regard, the goal of this study is to show that the water column length and the speed of discontinuity play an important role in predicting the distributions of flow variables, including peak values (maximum and minimum) as well as attenuation behaviors. Therefore, the Shock-Fitting approach, by facilitating the calculation of the free surface flow, allows calculating the speed of discontinuity that produces a more precise equation for calculating the water column length.

For this purpose, a closed conduit transient flow will be solved by a Shock-Fitting approach and solutions will be compared to the solutions of the rigid column model and the modified Saint-Venant equations as well as the experimental data of Hatcher et al. (2015). The undertaken Shock-Fitting approach includes the rigid column model, applied to the upstream pressurized flow, in which the relevant governing equations are solved using the implicit backward Euler scheme and the Saint-Venant equations set applied to the downstream free surface flow, which is solved by the method of characteristics (MOC).

General Description

In the steady state condition, the water, supplied by a constant flow-rate (Q_i) from a reservoir with initial absolute pressure head (H_u), enters the pipeline in a pressurized regime at the upstream.

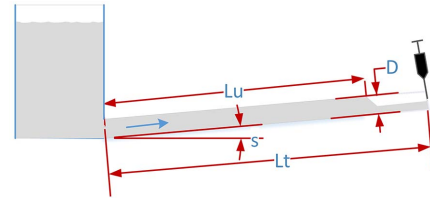


Fig. 1. Schematic diagram of entrapped air pocket in a closed conduit pressurized-free surface flow caused by blocking downstream end.

Somewhere along the pipeline the flow detaches from the pipe wall in which the free surface flow develops and discharges to the atmosphere at the downstream end at which it is assumed to be instantly blocked by a gate valve (Fig. 1). Following the experiment of Hatcher et al. (2015), the pipeline diameters are set as $D = 53$ mm and 102 mm with the total length $L_t = 10.7$ m and $L_t = 12$ m and adverse slopes $S = 2\%$ and $S = 1.3\%$, respectively. The pipe material is clear PVC with Manning roughness coefficient $n = 0.009$. Note that the kinematic viscosity of water is set as $\nu = 10^{-6}$ m²/s.

Governing Equations

As mentioned before, in the current Shock-Fitting approach the pressurized flow is simulated by the rigid column model and the free surface flow is calculated using the Saint-Venant governing equations set, solved by the MOC method. The Saint-Venant governing equations set have a form as (Chaudhry 2008)

$$\begin{aligned} \frac{\partial y}{\partial t} + V \frac{\partial y}{\partial x} + D_h \frac{\partial V}{\partial x} &= 0 \\ \frac{\partial V}{\partial t} + V \frac{\partial V}{\partial x} + g \frac{\partial y}{\partial x} &= g(S - S_f) \end{aligned} \quad (1)$$

where g is the gravitational constant ($g = 9.81$ m s⁻²) and y and V represent the flow depth and the velocity, respectively, varying along the pipe axis (x) with positive direction toward the downstream and varying along the time coordinate (t). The hydraulic depth (D_h) is calculated as $D_h = \frac{A}{B}$, where B is the water surface width and A is the cross-section area of the free surface flow. The parameter S is the pipe slope, assuming to be constant, and S_f is the friction slope calculated at each cross-section using the Chézy formula as

$$S_f = n^2 \frac{V^2}{R_h^{\frac{4}{3}}} \quad (2)$$

where R_h is the hydraulic radius.

The main concept of the rigid column model is to neglect the water compressibility so that the pressurized flow could be treated as a rigid column with a space-invariant velocity and acceleration. Thus, applying the momentum conservation law to this rigid column yields an equation as

$$\frac{dV_u}{dt} = g \frac{H_u - H_a}{L_u} + g \left[S - \left(\frac{f}{D} + \frac{K_{loss}}{L_u} \right) \frac{V_u |V_u|}{2g} \right] \quad (3)$$

where H_a is the air pocket absolute pressure head and V_u and L_u are the velocity and the length of the pressurized water column, respectively. The parameters f and K_{loss} are the Darcy friction factor and the summation of the local loss coefficients, respectively, which are assumed constant with given values $f = 0.025$ and $K_{loss} = 2.9$, similar to Hatcher et al. (2015) and Vasconcelos and Leite (2012). Note that this friction factor value, in the Moody

diagram, corresponds to a fully turbulent flow with the relative pipe roughness $\varepsilon = 0.002$. Moreover, the local head loss coefficient is set as $K_{loss} = 2.9$ in order to match experimental observations (Vasconcelos and Leite 2012).

The continuity equation applied to the pressurized column gives an equation for the rigid column length as

$$\frac{dL_u}{dt} = W_u \quad (4)$$

where W_u is the speed of the discontinuity between the pressurized and the free surface flows, also known as the celerity of wave fronts. Note that the upstream pressure head (H_u) is assumed to be constant and is calculated using the steady state condition as subsequently explained. Following Vasconcelos and Leite (2012) and Hatcher et al. (2015), the air absolute pressure head (H_a) is calculated using a polytropic process as

$$H_a \forall_a^k = cte \quad (5)$$

where k represents the polytropic coefficient, which is set as $k = 1.2$ (Vasconcelos and Leite 2012; Hatcher et al. 2015) and \forall_a is the air volume. The air volume change is caused by variations of depths in the free surface flow region and by variations of the length of the pressurized flow. Thus, by using the mass conservation law, the air volume rate could be calculated as

$$\frac{d\forall_a}{dt} = -V_1 A_1 + V_{i_{max}} A_{i_{max}} - (A - A_1) \frac{dL_u}{dt} \quad (6)$$

and substituting Eq. (4) into Eq. (6) results in

$$\frac{d\forall_a}{dt} = -V_1 A_1 + V_{i_{max}} A_{i_{max}} - (A - A_1) W_u \quad (7)$$

where the subscripts, 1 and i_{max} , denote the first and last mesh grid points of the free surface flow.

As mentioned before, in the Shock-Fitting approach the upstream pressurized flow and the downstream free surface flow are connected by the transient region. The celerity (W_u) is calculated using the mass conservation law applied to the transient region

$$W_u = \frac{AV_u - A_1 V_1}{A - A_1} \quad (8)$$

Note that the downstream end is assumed to be suddenly blocked, which implies $V_{i_{max}} = 0$. Therefore, substituting Eq. (8) into Eq. (7) yields

$$\frac{d\forall_a}{dt} = -AV_u \quad (9)$$

Boundary Conditions

It is assumed that the upstream reservoir maintains a constant water level and discharges a constant flowrate (Q_i) to the pipe.

At each time step, the water depth at the first node of the free surface flow (y_1) is calculated by interpolating the solutions in the other grid points. By using the method of characteristics, Fig. 2 illustrates that the velocity at the first grid point of the free surface flow (V_1) is calculated using the negative characteristic line originated from somewhere between the first and the second grid points of the free surface flow, as explained in the section "Numerical Simulations." In addition, Fig. 2 shows that only the positive characteristic line intersects the downstream boundary. Therefore, the relevant compatible equation to the positive characteristic line

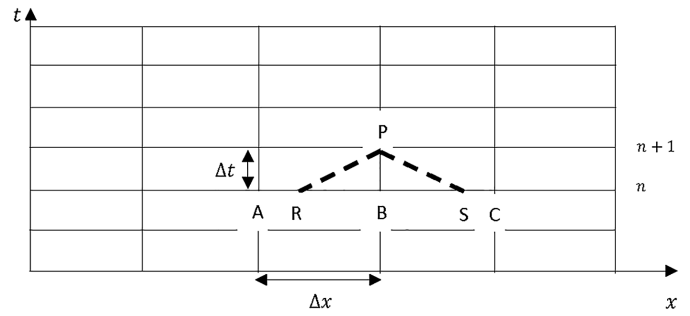


Fig. 2. Characteristic lines in a computational mesh.

originated from a point between the last grid and the one before is used to calculate the water depth in the last grid point ($y_{i_{max}}$) at the time level $n + 1$. Note that for this grid point the velocity is zero ($V_{i_{max}} = 0$).

Initial Conditions

With respect to the initial conditions, the first challenge is to find the profile of the free surface flow depth in the steady state condition. Alves et al. (1993) studied the drift velocity of an air bubble in an inclined liquid column and calculated the surface profile for different inclination angles, including the horizontal one. Further details are referred to Benjamin (1968) and Alves et al. (1993) and here it is only mentioned that the surface profile with zero inclination angle is taken as the steady state solution of the free surface flow because the undertaken slopes in this study are not so steep. Therefore, so far, the initial water surface elevations, $y_i(x_i)$ at each location (x_i) are calculated. The initial air pocket volume is calculated using the following formula,

$$\forall_a^0 = A(L_t - L_u^0) - \int_{L_u}^{L_t} A_f(x) dx \quad (10)$$

where \forall_a^0 denotes the initial air volume and L_u^0 is the initial rigid column length and $A_f(x)$ represents the cross-section area of the free surface flow at a location x . Following Hatcher et al. (2015), the initial air pocket volume is set to a certain amount and by using Eq. (10) the initial pressurized water column length (L_u^0) is changed manually such that the value of the initial air volume is achieved.

The initial velocity, at each cross-section, $V_i^0(x_i)$, can be calculated using the continuity equation as

$$Q_i = V_i^0(x_i) A_f(x_i) \quad (11)$$

With respect to the pressurized column, the initial velocity (V_u^0) is calculated through

$$Q_i = V_u^0 A \quad (12)$$

In order to calculate the initial absolute pressure head (H_u^0), the Bernoulli equation is solved from any point in the pressurized flow to a point in which the pressurized flow detaches from the wall, since this detachment implies zero velocity. Therefore

$$H_u^0 = H_a^0 - (1 - K_{loss}) \frac{V_u^0 |V_u^0|}{2g} + L_u^0 \left[-S + \left(\frac{f}{D} + \frac{K_{loss}}{L_u^0} \right) \frac{V_u^0 |V_u^0|}{2g} \right] \quad (13)$$

where H_a^0 is the initial air pressure head, which set as $H_a^0 = H_{atm}$.

Numerical Simulations

The Saint-Venant equations set of the free surface flow is solved using the MOC method, which preserves the first order of accuracy. To find dependent variables in time-space coordinates, this method transforms the governing Eq. (1) into two ordinary differential equations (ODEs) called compatibility equations that can be integrated along the characteristic lines. Further details of this method could be found in reference books (Chaudhry 2008). The compatibility equations of Eq. (1) are as

$$\frac{DV}{Dt} - \frac{gDy}{c} \frac{Dy}{Dt} = g(S - S_f) \quad (14)$$

$$\frac{DV}{Dt} + \frac{gDy}{c} \frac{Dy}{Dt} = g(S - S_f) \quad (15)$$

where c denotes the gravity wave speed ($c = \sqrt{gA/B}$). Note that derivatives in terms of the independent variables (x, t) have been changed to a derivative along the characteristic lines. Therefore

$$\frac{D}{Dt} = \frac{\partial}{\partial t} + \frac{\partial}{\partial x} \frac{dx}{dt} \quad (16)$$

where the positive and negative characteristic lines, corresponding to Eqs. (14) and (15) could be found, respectively, as follows

$$\frac{dx}{dt} = V - c \quad (17)$$

$$\frac{dx}{dt} = V + c \quad (18)$$

The numerical solution of the compatibility equations can be found using a finite difference computational mesh depicted in

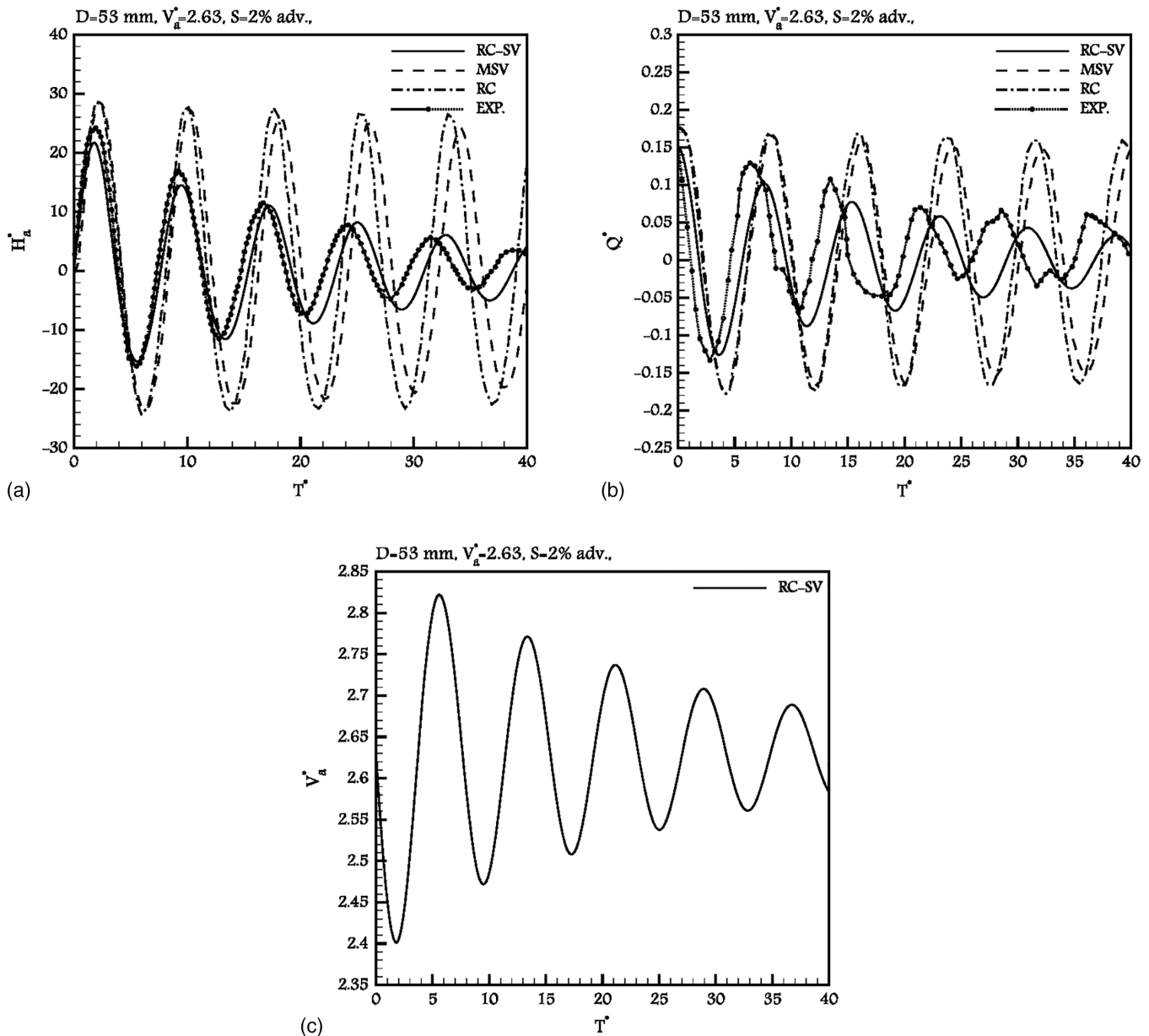


Fig. 3. (a) Distribution of nondimensional air pressure head; (b) discharge flowrate; and (c) air volume, calculated for case with $D = 53$ mm, $V_{a,0}^* = 2.63$, and $Q_0^* = 0.15$. Shock-Fitting approach (solid), modified Saint-Venant equations (dashed), rigid column model (dash dot), and experimental data (circled).

Fig. 2. As illustrated in Fig. 2, unknown variables at a time level $(n + 1)$ for a grid point (P) can be calculated using solutions at R and S , corresponding to a time level (n) . As can be seen, characteristic lines do not intersect time lines at the grid points A and B . Therefore, solutions at R and S need to be interpolated using solutions in other grid points. Note that in this paper a linear interpolation technique has been utilized. The discrete equations can then be written as follows (Chaudhry 2008)

$$V_p = D_q - \frac{g}{c_R} y_P \quad (19)$$

$$V_p = D_n + \frac{g}{c_S} y_P \quad (20)$$

where

$$D_q = V_R + \frac{g}{c_R} y_R + g(S - S_f)_R \Delta t \quad (21)$$

$$D_n = V_S - \frac{g}{c_S} y_S + g(S - S_f)_S \Delta t \quad (22)$$

where

$$\varphi_R = \varphi_B + CFL(\varphi_A - \varphi_B) \quad (23)$$

$$\varphi_S = \varphi_B + CFL(\varphi_C - \varphi_B) \quad (24)$$

where φ could be either V or y . Note that Δt represents the time step increment that is calculated using the Courant-Friedrichs-Lewy (CFL) condition. This condition for a free surface flow is as

$$CFL = [\max(V) + \max(c)] \frac{\Delta t}{\Delta x} \quad (25)$$

where \max denotes the maximum absolute value.

The governing equations of the pressurized flow [Eqs. (3) and (4)] and of the air pocket volume change [Eq. (9)] are solved using the backward Euler scheme, which is an implicit scheme with the first order of accuracy. Considering a general ODE problem as

$$\frac{d\psi}{dt} = f(\psi) \quad (26)$$

where ψ is any dependent variable. The backward Euler scheme applied to Eq. (26) yields a discrete formula as

$$\psi^{n+1} = \psi^n + \Delta t f(\psi^{n+1}) \quad (27)$$

where the superscripts indicate the time levels.

The air pocket pressure head, Eq. (5), at the time level $n + 1$ is calculated as

$$H_a^{n+1} (\nabla_a^{n+1})^k = H_a^n (\nabla_a^n)^k \quad (28)$$

Afterward, the celerity of the wave front in the transient region at each time level will be calculated using Eq. (8) as

$$W_u^{n+1} = \frac{AV_u^{n+1} - A_1 V_1^{n+1}}{A - A_1} \quad (29)$$

It is worth mentioning that due to the implicit time integration scheme, an iterative approach is needed, in which the residuals of all discrete equations, solved by backward Euler scheme at each time level, were imposed to converge up to a certain tolerance ($Tol = 10^{-15}$). Note that this tolerance is the smallest one that could be achieved during the calculations.

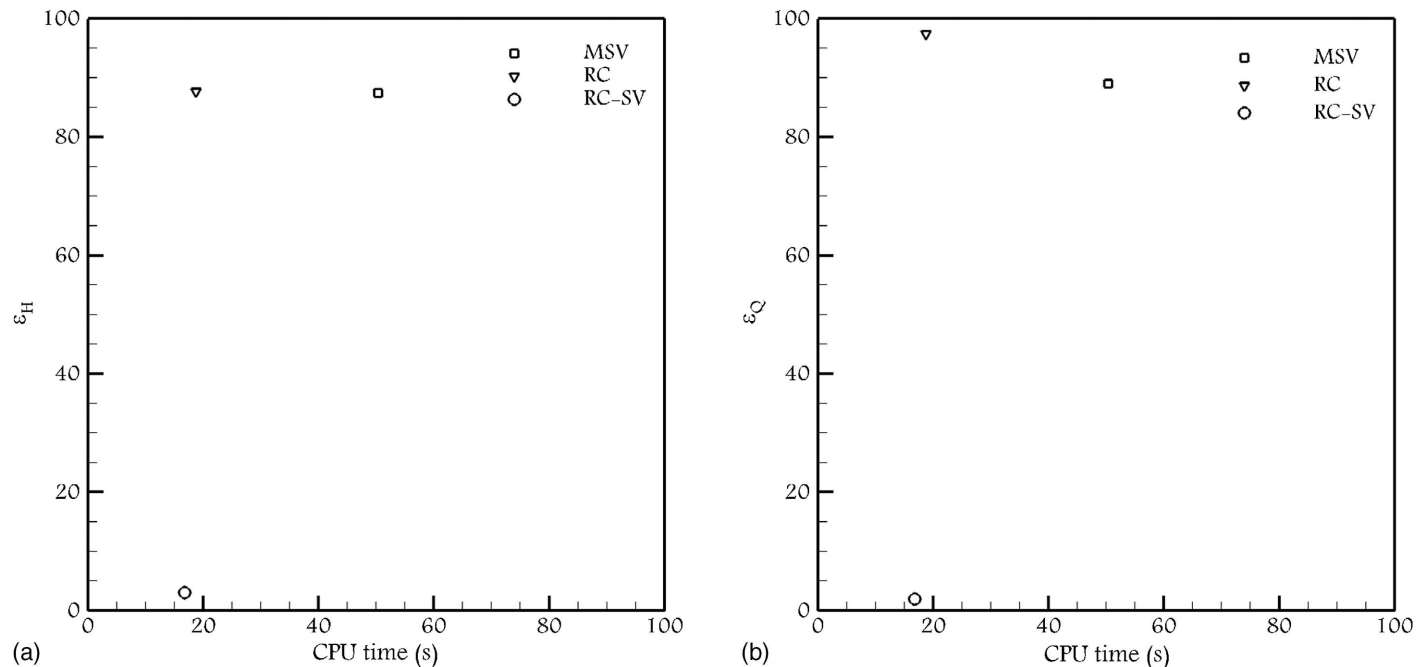


Fig. 4. (a) Numerical error of pressure head (ε_H) and (b) flowrate (ε_Q) in terms of CPU time usage, for MSV (square), RC (gradient), and RC-SV (circle), associated with Fig. 3.

Linear Stability Analysis

The purpose of a linear stability analysis is to analytically show how solutions propagate within a time coordinate. Although the behavior of solutions of nonlinear equations is not expected to be fully explained by this linear analysis, it still can provide general informative descriptions. In this study, the governing equations include the momentum [Eq. (3)], the continuity [Eq. (4)], the polytropic process [Eq. (5)], and the mass conservation law applied to the air pocket [Eq. (9)]. Note that the friction loss term in the momentum equation is neglected, since this term is nonlinear and its linearization unnecessarily makes the analysis complicated. The momentum equation is then simplified as

$$L_u \frac{dV_u}{dt} = -g(H_a - H_u) \quad (30)$$

The continuity that provides an equation for the water column length variation is already linear and helps to reform Eq. (30) as

$$\frac{dL_u V_u}{dt} = -g(H_a - H_u) + V_u W_u \quad (31)$$

In order to retrieve the new variable ($L_u V_u$) in the right-hand side (RHS) of Eq. (31), this equation is rearranged as

$$\frac{dL_u V_u}{dt} = -g(H_a - H_u) + \frac{W_u}{L_u} L_u V_u \quad (32)$$

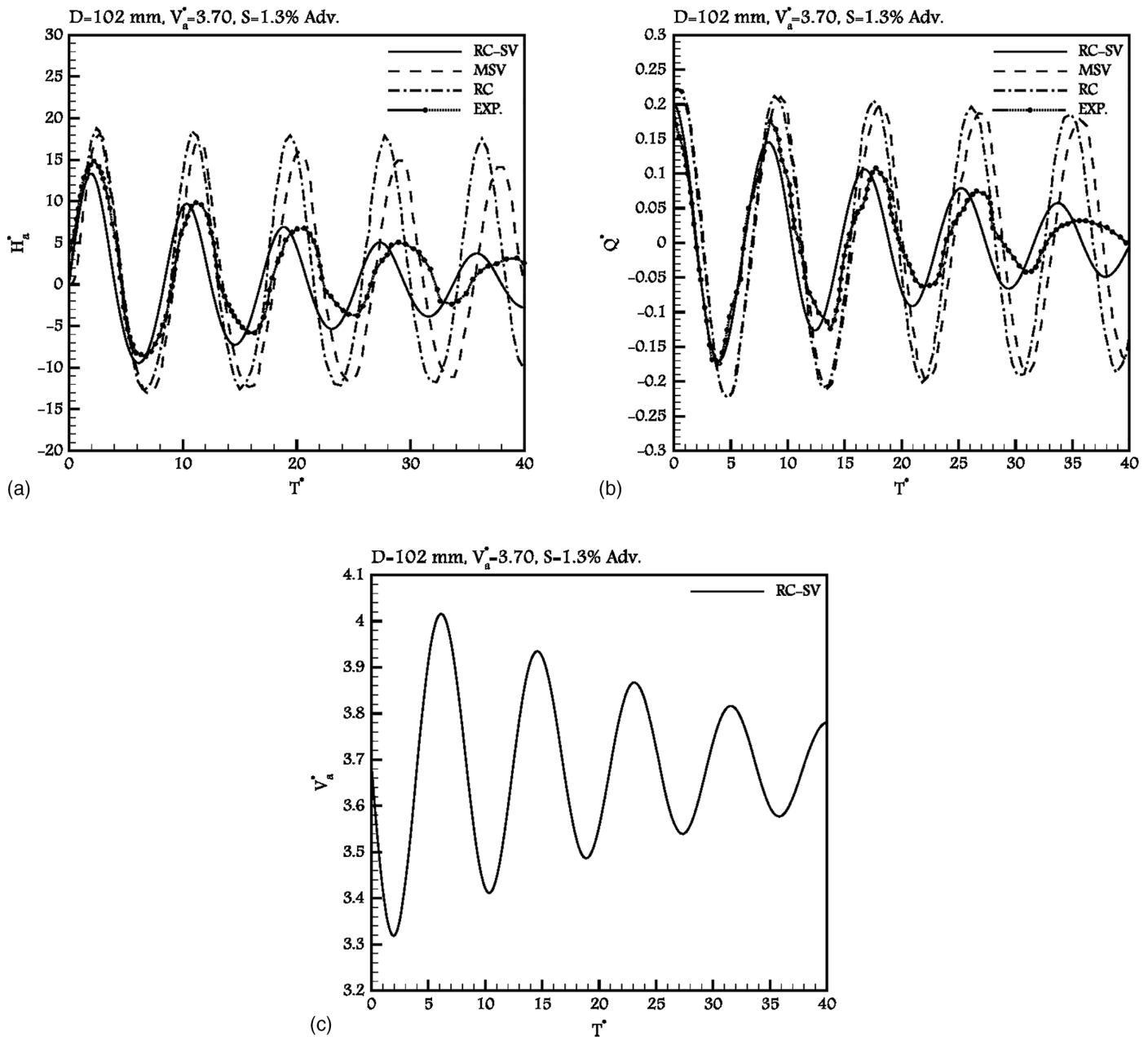


Fig. 5. (a) Distribution of nondimensional air pressure head; (b) discharge flowrate; and (c) air volume, calculated for case with $D = 102$ mm, $V_{a,0}^* = 3.70$, and $Q_0^* = 0.2$. Shock-Fitting approach (solid), modified Saint-Venant equations (dashed), rigid column model (dash dot), and experimental data (circled).

In this equation it is assumed that the variation of the coefficient W_u/L_u could be considered independent from the other variables. The polytropic process Eq. (5), after taking time derivative of both sides, could be linearized as

$$\frac{dH_a}{dt} + k \frac{H_a^0}{V_a^0} \frac{dV_a}{dt} = 0 \quad (33)$$

The mass conservation of the air pocket [Eq. (9)] simplifies [Eq. (9)] as

$$\frac{dH_a}{dt} = k \frac{H_a^0}{V_a^0} A V_u \quad (34)$$

and it is further simplified as

$$\frac{dH_a}{dt} = k \frac{H_a^0}{V_a^0} \frac{A}{L_u} L_u V_u \quad (35)$$

Thus the linearized governing equations are Eqs. (32) and (35) that can be presented in a vector form as

$$\frac{d\vec{F}}{dt} = \mathbf{G}\vec{F} + \vec{S} \quad (36)$$

where

$$\vec{F} = \begin{Bmatrix} L_u V_u \\ H_a \end{Bmatrix}, \quad \vec{S} = \begin{Bmatrix} gH_u \\ 0 \end{Bmatrix} \quad \text{and} \quad \mathbf{G} = \begin{bmatrix} \frac{W_u}{L_u} & -g \\ k \frac{H_a^0}{V_a^0} \frac{A}{L_u} & 0 \end{bmatrix} \quad (37)$$

Note that for the purpose of stability analysis the homogenous solutions of Eq. (36), also known as general solutions, are sufficient. The Eigen decomposition method gives the general solutions as an exponential function ($e^{\lambda t}$), in which λ is an eigenvalue. The analytical stability function (\mathbf{R}_a), defined as the ratio of the analytical solutions in two consecutive time steps, can be found as

$$\vec{F}^{n+1} = \mathbf{R}_a \vec{F}^n \quad (38)$$

where

$$\mathbf{R}_a = \begin{bmatrix} e^{\lambda_1 \Delta t} & 0 \\ 0 & e^{\lambda_2 \Delta t} \end{bmatrix} \quad (39)$$

where

$$\lambda_{1,2} = \frac{W_u}{2L_u} \pm \frac{1}{2} \sqrt{\frac{W_u^2}{L_u^2} - 4k \frac{gH_a^0}{V_a^0} \frac{A}{L_u}} \quad (40)$$

Two important remarks with respect to the analytical solutions of the linearized equations, which are related to the forms of the eigenvalues, Eq. (40); first, the experimental work of Hatcher et al. (2015) reveals that the solutions of the air pocket entrapment in a closed conduit transient flow propagate as a sinusoidal function through the time coordinate. With respect to the analytical solutions of the linearized governing equations, the sinusoidal function needs the term inside the square root in the RHS of Eq. (40) to be negative in order to produce a complex number. As can be seen in Eq. (40), the sign of the term inside the square root depends on the initial values of the flow variables, more dominantly, the initial air volume and the initial water column length. This dependency could result in a weak stability for the Shock-Fitting approach.

Second, the magnitude of the analytical stability function shows how the analytical solution attenuates through the time coordinate. It can be realized that this magnitude is

$$|\mathbf{R}_a| = e^{W_u \Delta t / 2L_u} \quad (41)$$

This equation indicates that the Shock-Fitting approach is able to predict the attenuation because of the celerity and the water column length; however, it depends on the choice of the time step that is related to the time integration scheme. Thus, it is required to find the numerical stability function of the backward Euler scheme.

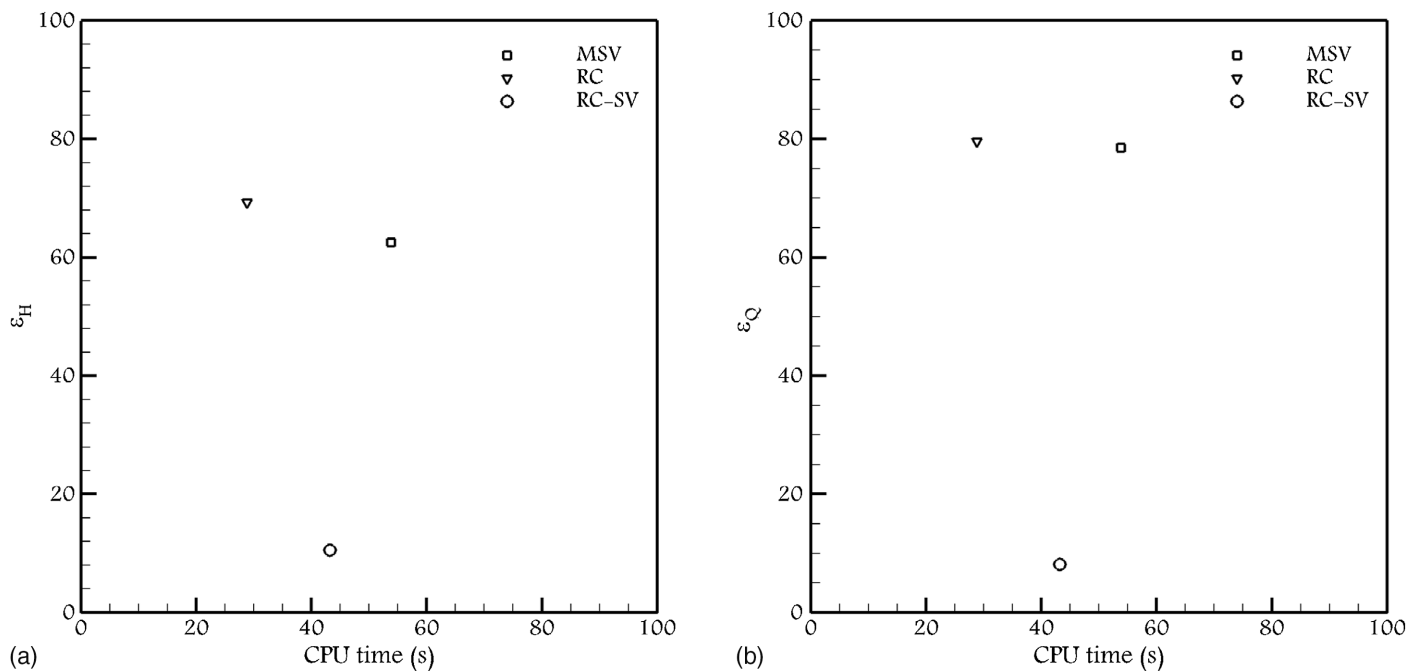


Fig. 6. (a) Numerical error of pressure head (ε_H) and (b) flowrate (ε_Q) in terms of CPU time usage, for MSV (square), RC (gradient), and RC-SV (circle), associated with Fig. 5.

The numerical stability function, defined as the ratio of the numerical solutions in two consecutive time steps, of the backward Euler scheme ($\mathbf{R}_{B.E.}$) applied to Eq. (36) can be found as

$$\mathbf{R}_{B.E.} = (\mathbf{I} - \Delta t \mathbf{G})^{-1} \quad (42)$$

where \mathbf{I} is the unit matrix. Here again, the solutions are in exponential form and the magnitude of the stability function is

$$|\mathbf{R}_{B.E.}| = e^{\left(\frac{1 - W_u \Delta t / (2L_u)}{(1 - W_u \Delta t / L_u) + k(h_{a,0} / \nabla_{a,0})(A/L_u)g\Delta t^2} \right)} \quad (43)$$

This equation indicates that the backward Euler scheme is able to predict the attenuation and it is affected by the size of time step.

Results and Discussions

In this section, the Shock-Fitting approach will be used to calculate the solutions in several cases with different ranges of initial air pocket volumes and initial flowrates, in order to examine the performance of this approach in practices. Note that the time step size is limited by the CFL condition in Eq. (25), which is set to 0.9.

The results of the Shock-Fitting approach, hereafter called RC-SV representing the rigid column model applied to the pressurized flow and the Saint-Venant equations applied to the free surface flow, is compared to the experimental data of Hatcher et al. (2015), called EXP, as well as their numerical solutions calculated by the rigid column model, called RC, and the modified Saint-Venant equations solved by MOC method, called MSV. It is worthwhile to mention that the MSV, due to taking the water compressibility and pipe elasticity into account, has an ability to calculate the pressure head variation implying that the flow is able to restore potential

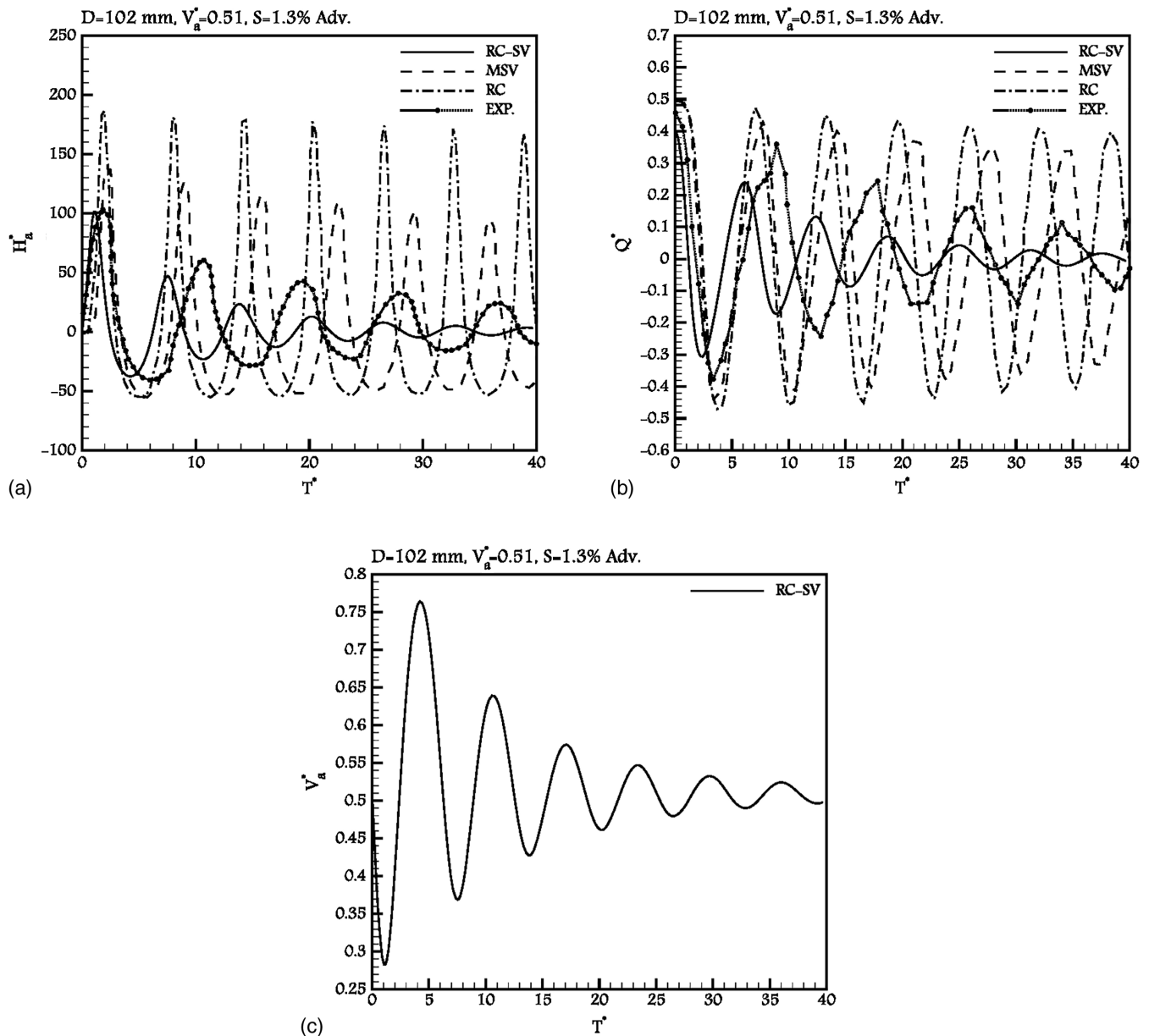


Fig. 7. (a) Distribution of nondimensional air pressure head; (b) discharge flowrate; and (c) air volume, calculated for case with $D = 102$ mm, $\nabla_{a,0}^* = 0.51$, and $Q_0^* = 0.4$. Shock-Fitting approach (solid), modified Saint-Venant equations (dashed), rigid column model (dash dot), and experimental data (circled).

energy (Karney 1990) besides the kinetic energy, which the rigid column model is able to calculate only.

In addition, to see how efficient each model is, the calculation costs and the magnitude of their numerical errors have been calculated for each example. The central processing unit (CPU) time usage shows the calculation cost, by which the ability of each model in converging to the solutions can be realized as well. Note that the CPU time usage was not calculated by Hatcher et al. (2015), thus, these models have been applied to those examples undertaken to calculate the CPU time. In this regard, the time step size, used for the rigid column model, was set as $\Delta t = 0.005$ s and the number of grid points, used in the Shock-Fitting approach and the modified Saint-Venant equations were set similarly. The CPU time usage is calculated as a time each model is taking to calculate the solutions for the entire calculation time period. It is worth mentioning that the calculations were done on a computer with an Intel 2 processor running Windows Server 2008 at 3.47 GHz using 96.0 GB of RAM.

In order to show how the Shock-Fitting approach improves the accuracy of the solutions, the percentage of the numerical error of each model was calculated as

$$\varepsilon_{\varphi} = \frac{|\sum |\varphi_N|/n_N - \sum |\varphi_E|/n_E|}{\sum |\varphi_E|/n_E} \times 100 \quad (44)$$

where ε represents the percentage of the numerical error, n represents the number of the time intervals and φ is either the pressure head or the flowrate and the subscripts N and E represent the numerical and experimental, respectively. Note that for the rigid column model and the modified Saint-Venant equations, using the work of Hatcher et al. (2015) the relevant numerical and experimental data of the pressure head and the flowrate variables were extracted by digitalizing the graphs provided in their article.

In the first case, the total length and diameter of the pipe are set as $L_t = 10.7$ m and $D = 53$ mm, respectively, which is adversely sloped with $S = 2.0\%$. The initial air pocket volume and the initial flowrate were set in nondimensional forms as $V_a^{*0} = 2.63$

and $Q^{*0} = 0.15$, where $V_a^* = V_a/D^3$ and $Q^* = Q/\sqrt{gD^5}$. Fig. 3(a) shows the distribution of the nondimensional air gauge pressure head, $H_a^* = (H_a - H_{atm})/D$; and the nondimensional flowrate (Q^*) [Fig. 3(b)] and the nondimensional air volume (V_a^*) are illustrated in terms of the nondimensional time variable ($T^* = t\sqrt{gD}/\sqrt[3]{V_a^{*0}}$) in Fig. 3(b) and Fig. 3(c), respectively.

As mentioned before, the water column length was adjusted manually so that the certain initial air volume value is found. The initial water column length for this example is found as $\frac{L_w}{L_t} \cong 0.96$. As can be seen from Fig. 3(a), the Shock-Fitting approach can capture the measured air pressure head more accurately than the RC and the MSV. This accuracy not only includes the pressure peak values (maximum and minimum values), but also, as expected from the solutions of the linearized equations, includes the attenuation of the solution through the time coordinate. Contrary to the RC model and the MSV, the Shock-Fitting approach slightly underestimates the first two peaks. The air volume distribution, calculated by the Shock-Fitting approach, is also provided in Fig. 3(c), to show that the behavior of the air volume is opposite of the air pressure head because of the polytropic process assumption.

Fig. 3(b) illustrates the distribution of the flowrate, calculated by the Shock-Fitting approach, which is compared to the experiment and the numerical results of Hatcher et al. (2015). Similar to the air pressure head distribution, the RC-SV could predict the attenuation of the flowrate and the first two peaks are underestimated, while they are similarly overestimated by the RC model and the MSV.

Fig. 4 illustrates the numerical errors calculated using Eq. (44) in terms of the CPU time usage. As can be seen, the RC-SV improves the accuracy of the solutions less expensively than the RC and the MSV models, which is also implying that this approach converges to the solution faster. It is worth mentioning that the numerical errors of the RC-SV are less than 5%, while those of RC and MSV models are more than 90%.

The performance of the Shock-Fitting approach is examined by solving another example with large initial air volume. In this example, the total length and diameter of the pipe are $L_t = 12.0$ m and $D = 102$ mm, which is adversely sloped with $S = 1.3\%$ and

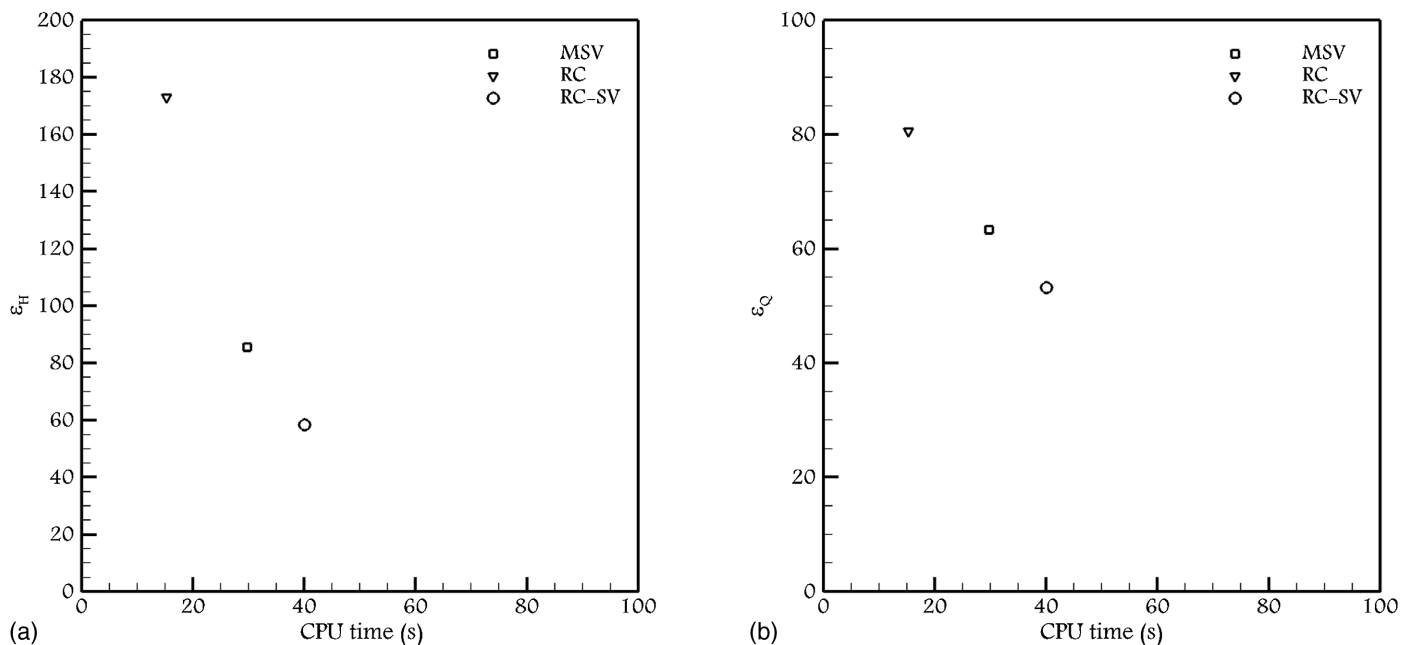


Fig. 8. (a) Numerical error of pressure head (ε_H); and (b) flowrate (ε_Q) in terms of CPU time usage, for MSV (square), RC (gradient), and RC-SV (circle), associated with Fig. 7.

the initial nondimensional air volume and flowrate are $V_a^{*0} = 3.70$ and $Q^{*0} = 0.20$. Note that the initial water column length has been found as $\frac{L_w}{L_t} \cong 0.90$. Fig. 5 illustrates (a) the distributions of the nondimensional air pressure head, (b) the nondimensional flowrate, and (c) the nondimensional air volume, calculated by the Shock-Fitting approach, which are compared to the results of the RC model and the MSV as well as the experimental data of Hatcher et al. (2015). Fig. 5 confirms that the Shock-Fitting approach outperforms the other models in calculating the maximum and minimum values as well as predicting the attenuation. These graphs also show that, similar to the previous example, the Shock-Fitting approach slightly underestimates the first maximum pressure value, while it is overestimated by the RC model and the MSV.

Fig. 6 illustrates the numerical errors in terms of CPU time usage and shows that after the RC model, the RC-SV is less expensive than the MSV model. However, in terms of the accuracy, the RC-SV provides more accurate solutions than the other two models.

As can be seen, the RC-SV approach generates numerical errors not more than 10%, which is significantly less than the corresponding values of RC and MSV models, which are more than 60%.

In order to further assess the performance of the Shock-Fitting approach, two more examples were solved in which the initial air pocket volumes are less and the initial flowrates are larger. Fig. 7 illustrates (a) the distributions of the nondimensional air pressure head, (b) the flowrate, and (c) the air volume in terms of the nondimensional time variable. In this case, the pipeline total length and diameter are set as $L_t = 12$ m and $D = 102$ mm, respectively, and it is adversely sloped with $S = 1.3\%$. The initial air pocket volume and the initial flowrate were set in nondimensional forms as $V_a^{*0} = 0.51$ and $Q^{*0} = 0.4$. Note that the initial water column length has been calculated as $\frac{L_w}{L_t} \cong 0.98$.

Similar to the previous examples, compared to the RC model and the MSV, the RC-SV provides a more accurate solution for the air pressure head, particularly the first two maximum and

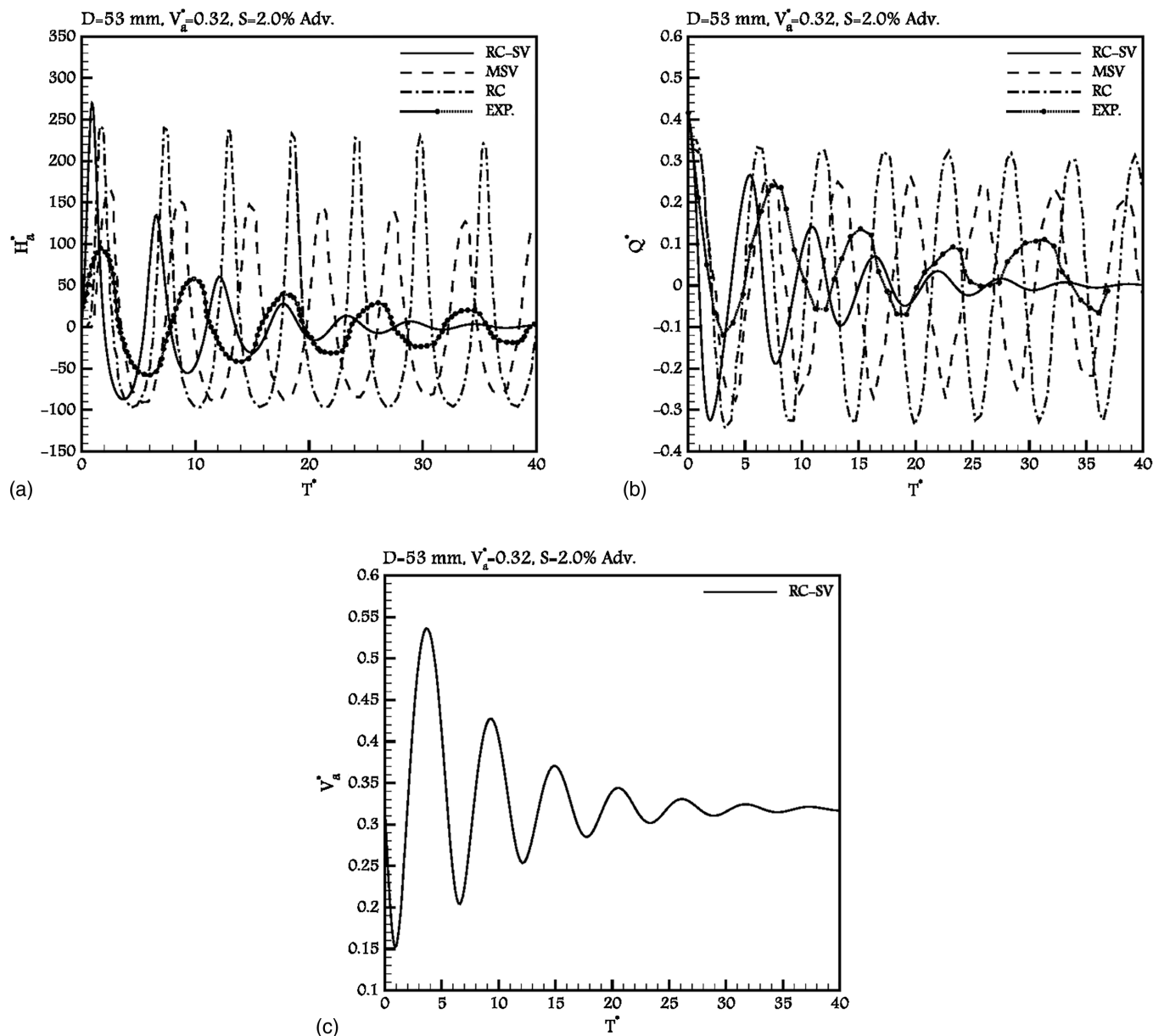


Fig. 9. (a) Distribution of nondimensional air pressure head; (b) discharge flowrate; and (c) air volume, calculated for case with $D = 53$ mm, $V_a^{*0} = 0.32$, and $Q_0^{*0} = 0.4$. Shock-Fitting approach (solid), modified Saint-Venant equations (dashed), rigid column model (dash dot), and experimental data (circled).

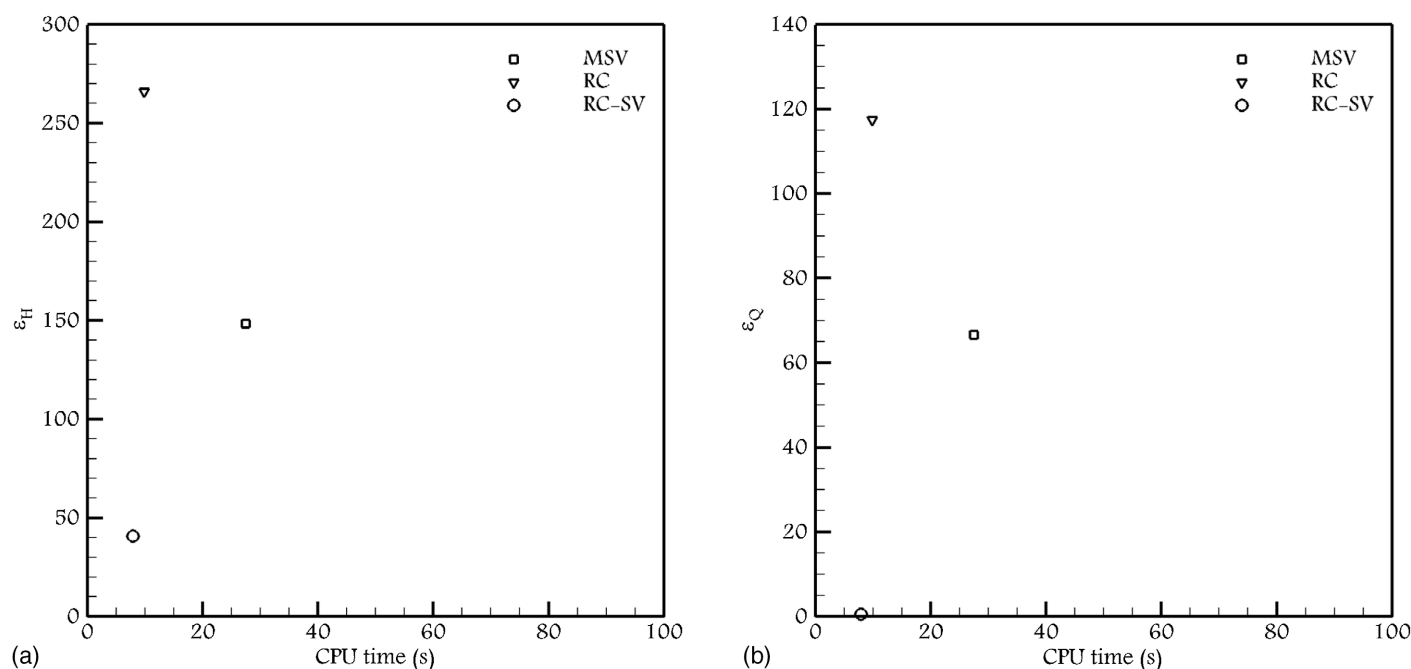


Fig. 10. (a) Numerical error of pressure head (ϵ_H) and (b) flowrate (ϵ_Q) in terms of CPU time usage, for MSV (square), RC (gradient), and RC-SV (circle), associated with Fig. 9.

minimum values. Here again the Shock-Fitting approach underestimates these peak values. This approach calculates the flowrate distribution more accurately, while the maximum and minimum values are underestimated. Moreover, the attenuated behavior is predicted for both variables, even though it is more rapid than the solutions in the previous examples. Looking at the magnitude of the numerical stability function in Eq. (43), the fast damping would be due to the small air pocket volume and large pressurized water column length. Note that the air volume rate, as shown in Fig. 7(c), confirms the ability of the Shock-Fitting approach in predicting the attenuation behavior.

Fig. 8 shows that for this example, the RC-SV approach is more expensive than the other two models. However, this approach improves the accuracy of the solutions of both the pressure head and the flowrate variables because the percentage of the numerical errors of the RC-SV approach is around 50% while these values for other models are significantly more than 60%. Note that the numerical error of the pressure head generated by the RC model is around 180%. This value implies a very large deviation of the RC model for cases with small initial air pocket sizes, particularly in calculating the pressure head.

For another example with a small initial air pocket, Fig. 9(a) illustrates the distributions of the nondimensional air pressure head, (b) the nondimensional flowrate, and (c) the nondimensional air volume. In this example, the pipeline total length and diameter were set as $L_t = 10.7$ m and $D = 53$ mm, respectively, which is adversely sloped with $S = 2.0\%$. The initial air pocket volume and the initial flowrate were set in nondimensional forms as $V_a^{*0} = 0.32$ and $Q^{*0} = 0.4$. In this example, the initial water column length has been found as $\frac{L_w}{L_t} \cong 0.99$.

Unlike the previous examples, in this example the first peak of the air pressure head is significantly overestimated by the Shock-Fitting approach. The reason, which certainly requires more investigation, could be due to very small air pocket volume that is identical to a very large pressurized water column length. Meanwhile, this overestimation could be linked to the weak unstable behavior of the Shock-Fitting approach. The first minimum pressure

head is calculated more accurately, similar to the previous examples. The attenuation is also predicted, even though the Shock-Fitting approach dampens faster than the experiment and faster than the cases with larger air pocket volumes. The upper-right graph shows that the distribution of the flowrate is calculated similar to the previous examples, although the first minimum value is overestimated. The attenuation is also predicted in the flowrate calculation similar to the previous examples as well as in calculating the air volume distribution in Fig. 9(c). Unlike the cases with large initial air volume, in which the rigid column model and the modified Saint-Venant equations behave similarly, as can be seen in Figs. 3 and 5, both Figs. 7 and 9 show that for cases with small initial air pocket volumes and large initial flowrates, the MSV improves the overestimation, compared to the RC model. Therefore, it could be mentioned that for the cases with small air pocket volume, which is identical to larger pressurized flow length, the elasticity of the pipe and the water compressibility, encompassed in the modified Saint-Venant equations by the acoustic wave speed, becomes more effective in calculations.

Fig. 10 shows that, for this example, the RC-SV takes less calculation cost than both RC and MSV models. Also, the numerical error of the Shock-Fitting approach is much less than the numerical error of the other two models. As can be seen from the numerical error of the pressure head, both RC and MSV models generate a large numerical error that is implying a poor behavior of both models in calculating the cases with small initial air pocket volume.

Fig. 11 shows the variation of the free surface flow depth at three different locations: at the first and the last grid points, and at the central section of the free surface flow, for all four preceding examples explained. Two important notes can be realized in Fig. 11; first, the water level at the first grid point as well as at the center, in all graphs, approaches a constant value after oscillations, which is implying an attenuation behavior of the free surface flow. The second note is, as shown in Fig. 11(d), the water level at the last grid point of this example, in which $D = 102$ mm, $V_a^* = 0.51$, and $S = -1.3\%$, becomes more than the pipe diameter and the flow touches the pipe crown. It means that the Saint-Venant equations

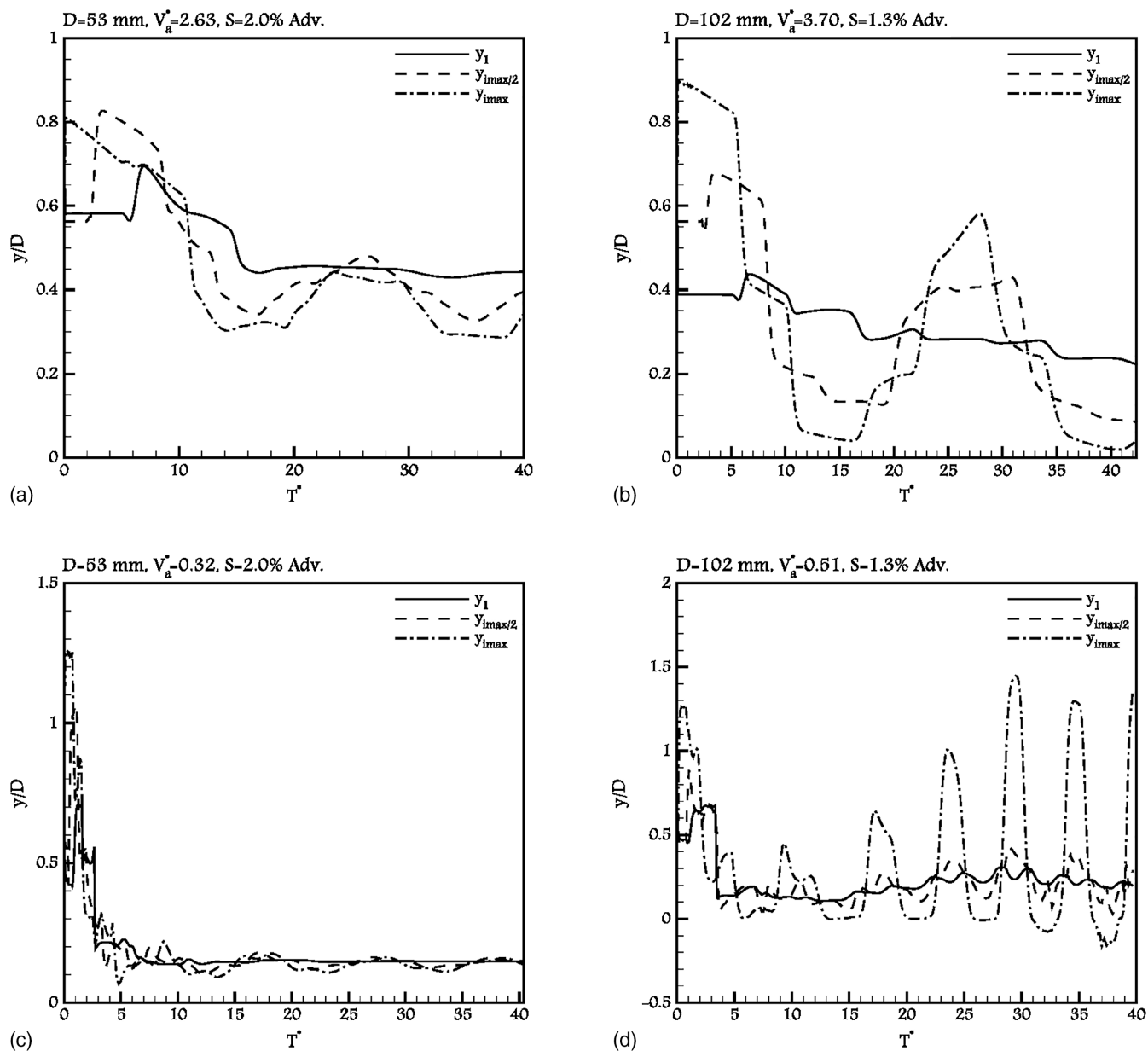


Fig. 11. Distribution of nondimensional free surface flow depth (y/D) in first grid point (solid), central grid point (dashed), and last grid point (dash dot), calculated by Shock-Fitting approach for the case with $D = 53$ mm and (a) $V_{a,0}^* = 2.63$, and (c) $V_{a,0}^* = 0.32$; and for the case with $D = 102$ mm and (b) $V_{a,0}^* = 3.70$ and (d) $V_{a,0}^* = 0.51$.

are no longer valid for the control volume around this grid point since flow at this section is no longer free surface type. Thus, as can be seen, the water level, calculated by the Saint-Venant equations, at this grid point does not exhibit an attenuation behavior. It is worth mentioning that this flow regime's change does not affect the calculation because it only shows creation of another rigid column at the downstream end with zero velocity, since the velocity at the last grid point is zero. Therefore, Eqs. (7) and (9) are still valid to calculate the variation of the air pocket volume.

Conclusion

In this paper, the Shock-Fitting approach has been studied in simulation of the air pocket entrapment caused by the complete obstruction of the downstream end of a closed conduit. The transient flow contains a pressurized flow at the upstream that

somewhere along the pipe at the downstream changes to a free surface flow. In the Shock-Fitting approach, the pressurized column is simulated using the rigid column model and the relevant governing equations have been solved by the backward Euler scheme. The free surface flow is modeled by the Saint-Venant equations and solved using the method of characteristics. Both flow regimes are linked with a transient region in which the discontinuity is contained.

The flow variables, the air pressure head, and the flowrate, have been calculated by the Shock-Fitting approach and the results were compared to the experimental data as well as the numerical results of the rigid column model and the modified Saint-Venant equations that were provided by Hatcher et al. (2015). Two cases have been studied in which large and small initial air pocket volumes and water flowrates have been considered in order to examine the ability of the Shock-Fitting approach in different conditions.

The linear stability analysis revealed the effects of the water column length and the celerity on the solutions. This analysis showed that the Shock-Fitting approach is able to calculate the attenuation behaviors of the physical solutions depending on the choice of the time integration scheme. Note that this attenuation was not predicted by the rigid column model, but it was slightly predicted by the modified Saint-Venant equations, as shown by Hatcher et al. (2015). Furthermore, the linear stability function showed that the Shock-Fitting approach has a potential of instability because the form of the solutions depends on the initial flow variables, particularly, the initial air pocket volume.

The Shock-Fitting approach was applied to different practical cases and it was found that this approach can improve the accuracy of the numerical solutions compared to the rigid column model and the modified Saint-Venant equations. It was shown that the Shock-Fitting approach, more effectively, predicts the first peak of the air pressure head, although it is slightly underestimated. The same behavior was found in calculating the flowrate, even though the Shock-Fitting approach seems to be more accurate in calculating the air pressure head.

Data Availability Statement

All data, models, or code that support the findings of this study are available from the corresponding author upon reasonable request.

Acknowledgments

The writers would like to express their gratitude to the Natural Sciences and Engineering Research Council of Canada (NSERC) for the financial support.

References

- Alves, I. N., O. Shoham, and Y. Taitel. 1993. "Drift velocity of elongated bubbles in inclined pipes." *Chem. Eng. Sci.* 48 (17): 3063–3070. [https://doi.org/10.1016/0009-2509\(93\)80172-M](https://doi.org/10.1016/0009-2509(93)80172-M).
- Benjamin, T. B. 1968. "Gravity currents and related phenomenon." *J. Fluid Mech.* 31 (2): 209–248. <https://doi.org/10.1017/S0022112068000133>.
- Bousso, S., M. Daynou, and M. Fuamba. 2013. "Numerical modeling of mixed flows in storm water systems: Critical review of literature." *J. Hydraul. Eng.* 139 (4): 385–396. [https://doi.org/10.1061/\(ASCE\)HY.1943-7900.0000680](https://doi.org/10.1061/(ASCE)HY.1943-7900.0000680).
- Bousso, S., and M. Fuamba. 2014. "Numerical and experimental analysis of the pressurized wave front in a circular pipe." *J. Hydraul. Eng.* 140 (3): 300–312. [https://doi.org/10.1061/\(ASCE\)HY.1943-7900.0000827](https://doi.org/10.1061/(ASCE)HY.1943-7900.0000827).
- Cardle, J. A., C. C. S. Song, and M. Yuan. 1989. "Measurements of mixed transient flows." *J. Hydraul. Eng.* 115 (2): 169–182.
- Chaiko, M. A., and K. W. Brinckman. 2002. "Models for analysis of water hammer in piping with entrapped air." *ASME J. Fluids Eng.* 124 (1): 194–204. <https://doi.org/10.1115/1.1430668>.
- Chaudhry, M. H. 2008. *Open-channel flow*. 2nd ed. New York: Springer.
- Cunge, J. A., and M. Wegner. 1964. "Numerical integration of Barre de Saint-Venant's flow equations by means of implicit scheme of finite differences." *Houille Blanche* 19 (1): 33–39. <https://doi.org/10.1051/lhb/1964002>.
- Fuamba, M. 2002. "Contribution on transient flow modelling in storm sewers." *J. Hydraul. Res.* 40 (6): 685–693. <https://doi.org/10.1080/00221680209499915>.
- Guo, Q., and C. C. S. Song. 1990. "Surging in urban storm drainage systems." *J. Hydraul. Eng.* 116 (12): 1523–1537. [https://doi.org/10.1061/\(ASCE\)0733-9429\(1990\)116:12\(1523\)](https://doi.org/10.1061/(ASCE)0733-9429(1990)116:12(1523)).
- Hamam, M. A., and J. A. McCorquodale. 1982. "Transient conditions in the transition from gravity to surcharged sewer flow." *Can. J. Civ. Eng.* 9 (2): 189–196. <https://doi.org/10.1139/l82-022>.
- Hatcher, T. M., A. Malekpour, J. G. Vasconcelos, and B. W. Karney. 2015. "Comparing unsteady modeling approaches of surges caused by sudden air pocket compression." *J. Water Manage. Model.* 23: C392. <https://doi.org/10.14796/JWMM.C392>.
- Karney, B. W. 1990. "Energy relations in transient closed-conduit flow." *J. Hydraul. Eng.* 116 (10): 1180–1196. [https://doi.org/10.1061/\(ASCE\)0733-9429\(1990\)116:10\(1180\)](https://doi.org/10.1061/(ASCE)0733-9429(1990)116:10(1180)).
- León, A. S. 2007. *Improved modeling of unsteady free surface, pressurized and mixed flows in storm-sewer systems*. Urbana, IL: Univ. of Illinois at Urbana-Champaign.
- León, A. S., M. S. Ghidaoui, A. R. Schmidt, and M. H. García. 2007. "An efficient finite-volume scheme for modeling water hammer flows." *J. Water Manage. Model.* 15: R227–21. <https://doi.org/10.14796/JWMM.R227-21>.
- León, A. S., M. S. Ghidaoui, A. R. Schmidt, and M. H. García. 2010. "A robust two-equation model for transient-mixed flows." *J. Hydraul. Res.* 48 (1): 44–56. <https://doi.org/10.1080/00221680903565911>.
- Li, J., and A. McCorquodale. 1999. "Modeling mixed flow in storm sewers." *J. Hydraul. Eng.* 125 (11): 1170–1180. [https://doi.org/10.1061/\(ASCE\)0733-9429\(1999\)125:11\(1170\)](https://doi.org/10.1061/(ASCE)0733-9429(1999)125:11(1170)).
- Li, J., and A. McCorquodale. 2001. *Modeling the transition from gravity to pressurized flows in sewers*. Orlando, FL: ASCE.
- Malekpour, A., and B. W. Karney. 2012. "Discussion of 'pressure surges following sudden air pocket entrapment in storm-water tunnels' by José G. Vasconcelos and Gabriel M. Leite." *J. Hydraul. Eng.* 140 (4): 1081–1089. [https://doi.org/10.1061/\(ASCE\)HY.1943-7900.0000818](https://doi.org/10.1061/(ASCE)HY.1943-7900.0000818).
- Martin, C. S. 1996. "Experiences with two-phase flow in fluid transients." In *Proc., 7th Int. Conf. on Pressure Surges*, 65–75. Bedford, UK: BHR Group.
- Politano, M., A. J. Odgaard, and W. Klecan. 2007. "Case study: Numerical evaluation of hydraulic transients in a combined sewer overflow tunnel system." *J. Hydraul. Eng.* 133 (10): 1103–1110. [https://doi.org/10.1061/\(ASCE\)0733-9429\(2007\)133:10\(1103\)](https://doi.org/10.1061/(ASCE)0733-9429(2007)133:10(1103)).
- Tijsseling, A. S., Q. Hou, and Z. Bozkus. 2019. "Rapid liquid filling of a pipe with venting entrapped gas: Analytical and numerical solutions." *J. Pressure Vessel Technol.* 141 (4): 041301. <https://doi.org/10.1115/1.4043321>.
- Trajkovic, B., M. Ivetic, F. Calomino, and A. D'Ippolito. 1999. "Investigation of transition from free-surface to pressurized flow in a circular pipe." *Water Sci. Technol.* 39 (9): 105–112. <https://doi.org/10.2166/wst.1999.0453>.
- Vasconcelos, J. G., and G. M. Leite. 2012. "Pressure surges following sudden air pocket entrapment in stormwater tunnels." *J. Hydraul. Eng.* 138 (12): 1081–1089. [https://doi.org/10.1061/\(ASCE\)HY.1943-7900.0000616](https://doi.org/10.1061/(ASCE)HY.1943-7900.0000616).
- Vasconcelos, J. G., and D. T. B. Marwell. 2011. "Innovative simulation of unsteady low-pressure flows in water mains." *J. Hydraul. Eng.* 137 (11): 1490–1499. [https://doi.org/10.1061/\(ASCE\)HY.1943-7900.0000440](https://doi.org/10.1061/(ASCE)HY.1943-7900.0000440).
- Vasconcelos, J. G., and S. J. Wright. 2007. "Comparison between the two-component pressure approach and current transient flow solvers." *J. Hydraul. Res.* 45 (2): 178–187. <https://doi.org/10.1080/00221686.2007.9521758>.
- Vasconcelos, J. G., S. J. Wright, and P. L. Roe. 2006. "Current issues on modeling extreme inflows in stormwater systems." In *Intelligent modeling of urban water systems, monograph 14*, edited by W. James, K. N. Irvine, E. A. Mc Bean, and R. E. Pitt. Guelph, ON, Canada: Computational Hydraulics International.
- Zhou, F., F. Hicks, and P. Steffler. 2004. "Analysis of effects of air pocket on hydraulic failure of urban drainage infrastructure." *Can. J. Civ. Eng.* 31 (1): 86–94. <https://doi.org/10.1139/l03-077>.